X-ray-induced molecular catapult: ultrafast dynamics driven by lightweight linkages

Oksana Travnikova, Victor Kimberg, Barbara Cunha de Miranda, Florian Trinter, Markus Schöffler, Stéphane Carniato, Tatiana Marchenko, Renaud Guillemin, Iyas Ismail, Gregor Kastirke, et al.

X-ray-induced molecular catapult: Ultrafast dynamics driven by light linkages

Oksana Travnikova,[*,†] Victor Kimberg,[‡] Barbara Cunha de Miranda,[†] Florian Trinter,[¶,§] Markus S. Schöffler,[‖] Stéphane Carniato,[†] Tatiana Marchenko,[†] Renaud Guillemin,[†] Iyas Ismail,[†] Gregor Kastirke,[‖] Maria Novella Piancastelli,[†] Till Jahnke,[⊥,#] Reinhard Dörner,[‖] and Marc Simon[†]

†*Sorbonne Université, CNRS, UMR 7614, Laboratoire de Chimie Physique-Matière et Rayonnement, F-75005 Paris, France*

‡*Department of Theoretical Chemistry and Biology, KTH Royal Institute of Technology, 10691 Stockholm, Sweden*

¶*FS-PETRA-S, Deutsches Elektronen-Synchrotron (DESY), D-22607 Hamburg, Germany*

§*Molecular Physics, Fritz-Haber-Institut der Max-Planck-Gesellschaft, D-14195 Berlin, Germany*

‖*Institut für Kernphysik, Goethe-Universität, D-60438 Frankfurt am Main, Germany*

⊥*European XFEL, D-22869 Schenefeld, Germany*

#*Max-Planck-Institut für Kernphysik, 69117 Heidelberg, Germany*

E-mail: oksana.travnikova@upmc.fr

Abstract

In our work, we demonstrate that X-ray photons can initiate a "molecular catapult" effect, leading to the dissociation of chemical bonds and the formation of heavy fragments within just a few femtoseconds. We reconstruct the momenta of fragments from a three-body dissociation in bromochloromethane using the ion pair average (IPA) reference frame, demonstrating how light atomic groups, such as alkylene and alkanylene, can govern nuclear dynamics during the dissociation process, akin to projectiles released by a catapult. Supported by *ab initio* calculations, this work highlights the crucial role of low-reduced-mass vibrational modes in driving ultrafast chemical processes.

TOC Graphic

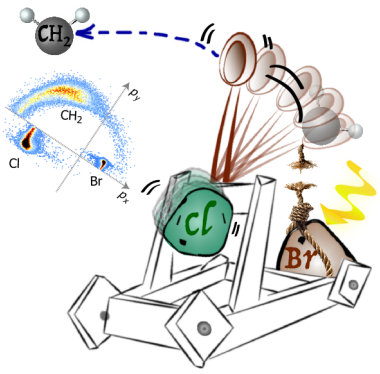

Absorption of an X-ray photon by a molecule may lead to excitation of an inner-shell electron to an anti-bonding molecular orbital, which then induces ultrafast nuclear dynamics and even causes dissociation of a chemical bond on just a few-femtosecond (fs) time scale (1 fs = 10^{-15} s). Ultrafast dissociation (UFD) is a phenomenon, when the breakage of molecular bonds occurs on the same time scale and, therefore, competes with electronic relaxation, which results in radiative or Auger decay emission from already dissociated fragments.[1–12] All in-depth studies of the UFD phenomenon used either diatomic molecules or a simple pseudo-diatomic description of UFD for polyatomic molecules, i.e., modeling the departing fragments as point masses and the dissociation along only one coordinate. This guided the previous studies of UFD to relatively light molecules, where the reduced mass of

dissociation allows the fragments to travel far enough to reach the complete breakage of the chemical bond during the very short core-hole lifetime.[13–18] For example, contrary to HCl, DCl, and CH_3Cl, UFD is quenched in repulsive core-excited intermediate states of the Cl_2 molecule owing to its high reduced mass.[3,19] Nevertheless, there were experimental observations of the UFD process preceding electronic relaxation in poly-chlorinated alkylenes and alkanylenes following resonant excitation of the $2p$ core electron to the anti-bonding molecular orbital from one of the Cl atoms.[20–22] However, the mechanisms, which would explain the possibility of UFD yielding heavy fragments on a few-fs time scale, are not yet understood. A recent X-ray spectroscopic study of 1-bromo-2-chloroethane [$Br(CH_2)_2Cl$] clearly demonstrated the limitation of modeling molecular dissociation, involving strongly repulsive intermediate states, as a simple one-dimensional bond elongation between two fragments.[23] In that previous work, it was suggested that bond breakages may be mediated by the internal motion of light linkages, which experience significant displacement in the very early stages of the photodissociation while the heavy atoms, such as halogens, remain nearly still. In this paper, we show that not only do the light bridges drive the dynamics, but they are also the first to be expelled from the molecule before its complete disintegration. Typically, halogenated organic molecules exhibit multiple normal vibrational modes characterized by low reduced masses, primarily driven by the motion of the lighter atom or group of atoms adjacent to the halogen in the dissociating chemical bond. A detailed description of this type of photo-induced nuclear dynamics requires consideration of multidimensional potential energy surfaces, which is a challenging task even for small polyatomic systems.[24]

In previous works, to overcome the problem of describing dissociation dynamics of alkyl halides on complex multidimensional surfaces, impulsive models rooted in classical mechanics were frequently employed.[25–28] These models simplify the dissociation process by assuming instantaneous dissociation of noninteracting atoms, where the repulsive force acts solely along the bond axis at the equilibrium geometry of the parent molecule. Energy partitioning between the photofragments is then determined by conservation of energy and angular

momentum, resulting in significant rotational excitations in the fragments. However, despite their usefulness in offering initial insights into the dissociation mechanisms of alkyl halides, these models have significant limitations. They neglect vibrational dynamics, long-range interactions, and complex fragmentation pathways. In general, impulsive models tend to overestimate the rotational energy in the molecular photofragments, in particular because they overlook vibrational excitations, such as bending and umbrella motions, which are likely important in all alkyl halide dissociations.[24,27] In our work, to support the conclusions derived from the experimental data analysis, we use *ab initio* theoretical methods, which incorporate vibrational normal modes, abstaining from the inclusion of impulsive models. This ensures a comprehensive understanding of the molecular behavior by emphasizing the pertinent aspects of *ab initio* theory, particularly highlighting the collective coupling of vibrational modes that govern the overall dynamics.

In this work, we performed cold target recoil ion momentum spectroscopy (COLTRIMS) measurements to 'capture' nuclear dynamics involved in the UFD process of strongly repulsive intermediate states using an example of Br $3d$ core-excited states of bromochloromethane (Br–CH_2–Cl, BCM) with a lifetime of $\tau \sim$7 fs. Following the absorption of a soft X-ray photon at two photon energies, above and below the Br $3d$ ionization threshold, corresponding to the bound Br $3d^{-1}$ and dissociative Br $3d^{-1}\sigma^*$ intermediate states, respectively, we focus on the $Br^+/CH_2^+/Cl^+$ fragmentation, which dominates all triple-ion dissociation channels.[29] By comparing the momentum distributions at these two photon energies, we attribute the observed variations to the nuclear dynamics in the dissociative core-excited state, which underlies the UFD process. This approach allows us to gain insights into the molecular dissociation mechanisms in dihalogenated alkylene molecules. Notably, Schmelz et al.[29] reported no significant difference in ion yields between the Br $3d^{-1}\sigma^*$ resonance and above ionization threshold for the BCM molecule. Therefore, the observed variations in ion momentum distributions between the resonance and continuum can be directly attributed to the different geometries of the core-excited and core-ionized intermediate states at the moment

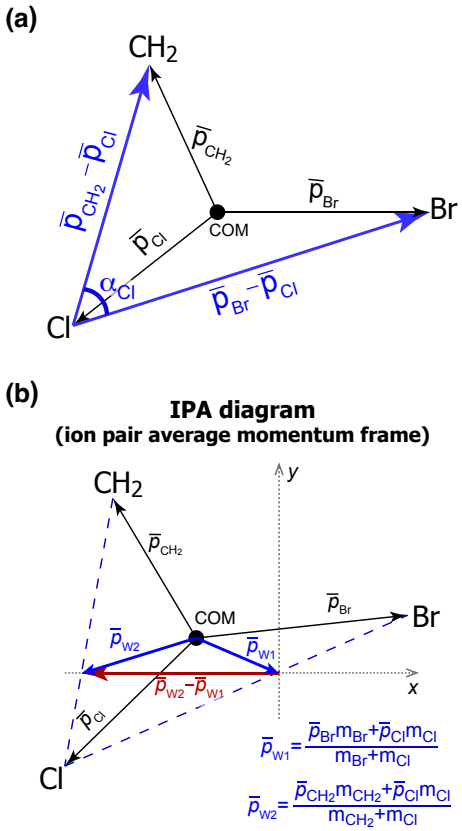

Figure 1: Schematic representation in a momentum space for (a) the angle $\angle\alpha_{Cl}$, which is an angle between two composite momentum vectors $(\bar{p}_{CH_2} - \bar{p}_{Cl})$ and $(\bar{p}_{Br} - \bar{p}_{Cl})$; (b) construction of momentum correlation diagrams in the IPA frame (mass-weighted ion-pair average momentum frame).

of electronic decay followed by rapid Coulomb explosion.

In this work, we focus on the primary dissociation channel, representing over 95% of all dissociation events of CH_2ClBr^{3+} into CH_2^+, Br^+, and Cl^+. There are significant differences between data recorded above the ionization threshold at 85 eV, where a bound core-ionized state is formed, and on the resonance at 70.3 eV, corresponding to the excitation of the Br $3d$ electron to the strongly repulsive anti-bonding molecular orbital.

We use the angle $\angle\alpha_{Cl}$ as an indicator of the CH_2 group's rotation, which precedes electronic relaxation leading to the formation of CH_2ClBr^{3+}. This highly charged intermediate then rapidly dissociates via Coulomb explosion. The angle $\angle\alpha_{Cl}$ is defined as the angle between two composite momentum vectors, namely those formed by the Cl^+–Br^+ and Cl^+–CH_2^+ ion pairs [see Fig. 1(a)]. From Fig. 2(a), we can see that the main dissociation pathway

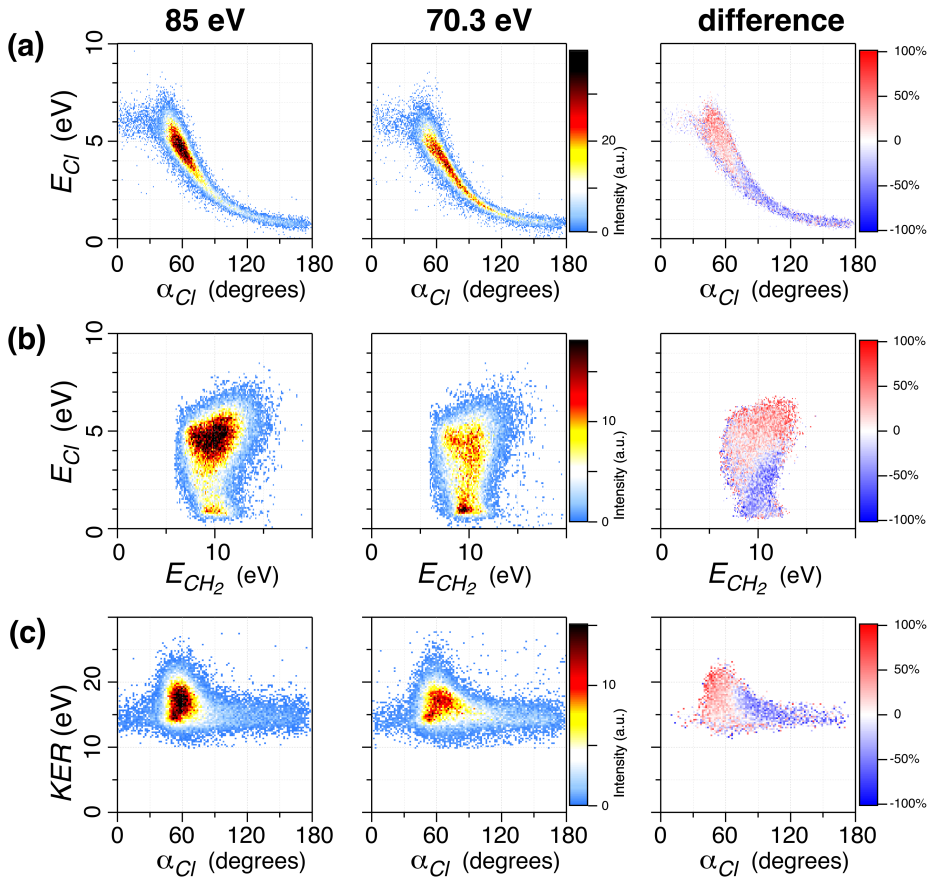

Figure 2: Correlation of ion energies for the dominant pathway pattern of CH_2ClBr^{3+} into CH_2^+ / Br^+ / Cl^+, measured in coincidence by our COLTRIMS setup. (a) Dependence of E_{Cl} on the angle $\angle\alpha_{Cl}$ at 85 eV and 70.3 eV, as well as their normalised difference plot. (b) Correlation of E_{Cl} vs. E_{CH_2} at 85 eV and 70.3 eV, and the normalised difference plot. (c) Dependence of the kinetic energy release (KER) on the angle $\angle\alpha_{Cl}$ at 85 eV and 70.3 eV, and the normalised difference plot. Prior to post-treatment data filtering, the data were normalised to the total integrated event count for photon energies 85 and 70.3 eV, respectively. The normalised difference corresponds to $(I_{85eV} - I_{70.3eV})/(I_{85eV} + I_{70.3eV})$.

indicates an increase of $\angle\alpha_{Cl}$, accompanied by a decrease of the energy of the Cl^+ ion (E_{Cl}), approaching near-zero values when $\angle\alpha_{Cl}$ reaches 180°. The angle $\angle\alpha_{Cl} = 180°$ corresponds to the linear geometry CH_2–Cl–Br, where the Cl atom does not acquire momentum during a Coulomb explosion because it is positioned between the CH_2 and Br atoms, both of which gain opposite momenta.

Rotational motion of the CH_2 group is manifested by significant counts at $\angle\alpha_{Cl}$ values greater than 70° and is particularly pronounced in the middle panel of Fig. 2(a), which is

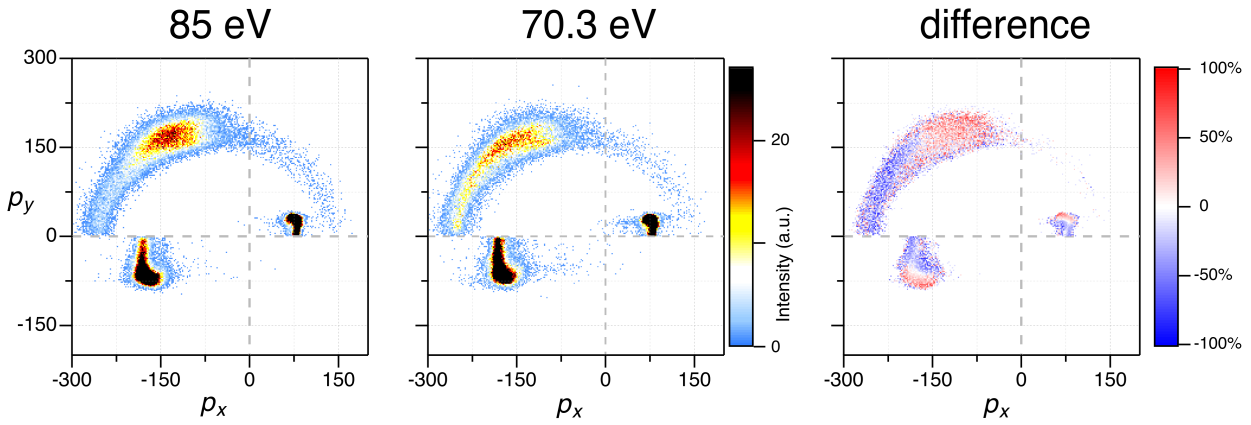

Figure 3: Momentum correlation analysis in the IPA reference frame for CH_2ClBr^{3+} dissociating into CH_2^+ / Br^+ / Cl^+ for 85 eV photon energy, corresponding to Br $3d$ ionization (left); for 70.3 eV photon energy, corresponding to the Br $3d \rightarrow \sigma^*$ resonant excitation (middle); and the normalised difference plot (right). The plots in the left and middle panels are normalised to the total integrated event count for 85 and 70.3 eV prior to filtering in the post-treatment of the data, respectively. The normalised difference corresponds to $(I_{85eV} - I_{70.3eV})/(I_{85eV} + I_{70.3eV})$.

even more clearly highlighted in the difference plot. This suggests that the ultrafast nuclear dynamics involving dissociation of the CH_2Br bond are more prominent at 70.3 eV photon energy, corresponding to the resonant excitation of the Br $3d$ electron into the anti-bonding LUMO. This observation aligns well with the dissociative nature of the Br $3d^{-1}\sigma^*$ core-excited state.

Figure 2(b) shows the correlation of the Cl^+ and CH_2^+ ion energies (E_{Cl}, E_{CH_2}). It is worth noting that E_{CH_2} remains nearly constant across the entire range of E_{Cl} and thus of $\angle\alpha_{Cl}$ angles, indicating that the dissociation of the CH_2 moiety is largely independent of the other dynamics occurring in the molecule. Nevertheless, an increase of $\angle\alpha_{Cl}$, leading to a gradual reduction of E_{Cl}, is clearly accompanied by a slight decrease of E_{CH_2}. Moreover, the total kinetic energy release (KER) of the CH_2ClBr molecular system also undergoes a slight decrease concurrently with the rotation of the CH_2 group [Fig. 2(c)]. This suggests that the entire molecule expands over time, as longer durations are required to achieve larger $\angle\alpha_{Cl}$ angles. In the left panel of Fig. 2(b), corresponding to the data recorded above the ionization threshold, this specific channel corresponding to the decrease of E_{Cl} and therefore increase

of $\angle\alpha_{Cl}$ is faintly observed and appears only weakly.

To "visualize" nuclear dynamics of all the detected ions, produced after a three-body dissociation, we have adapted Newton diagrams, which allow to discern the dynamics, emphasizing the correlated motions of the particles involved. Newton diagrams are graphical representations used to analyze the momenta of several fragments produced in a dissociation event. Each vector's length signifies the particle's momentum, while the angle indicates its direction relative to a chosen reference frame. While commonly used Newton diagrams are constructed in the center-of-mass frame (COM) of the system, they require fixing the momentum of one of the particles relative to which the momenta of the remaining particles are calculated.[30] Therefore, in some cases Newton diagrams can be misleading, especially if structural changes in molecular geometry have a strong influence on the momentum of the chosen reference. Previously, to avoid restricting single ions to a fixed direction in a molecular frame, the concept of sum and difference momenta was employed.[31,32] In our work, we establish a reference frame that incorporates the inherent dynamics of all dissociating partners by constructing ion momenta within the frame of the mass-weighted average momenta of the two selected ion pairs (IPA), which is schematically depicted in Fig. 1(b). This approach also takes into account the substantial differences in the masses of the fragments, which have a profound influence on the dynamics. In our IPA frame, the x axis is selected along the composite momentum vector $\bar{p}_{W2} - \bar{p}_{W1}$, where $\bar{p}_{W1}$ and $\bar{p}_{W2}$ are the mass-weighted average momenta of selected ion pairs:

$$\bar{p}_{W1} = \frac{\bar{p}_{Br} m_{Br} + \bar{p}_{Cl} m_{Cl}}{m_{Br} + m_{Cl}}; \quad \bar{p}_{W2} = \frac{\bar{p}_{CH_2} m_{CH_2} + \bar{p}_{Cl} m_{Cl}}{m_{CH_2} + m_{Cl}}. \tag{1}$$

The momenta of the three dissociating particles are calculated relative to $\bar{p}_{W1}$ and $\bar{p}_{W2}$. Here, we have chosen the Cl^+–CH_2^+ and Cl^+–Br^+ ion pairs, that form the angle $\angle\alpha_{Cl}$, and the momenta of the CH_2^+, Cl^+, and Br^+ ions are constructed relative to the mass-weighted average momentum vectors of these ion pairs. The resulting momentum correlation diagrams for CH_2ClBr are shown in Fig. 3 for the main dissociation pathway at 85 and 70.3 eV,

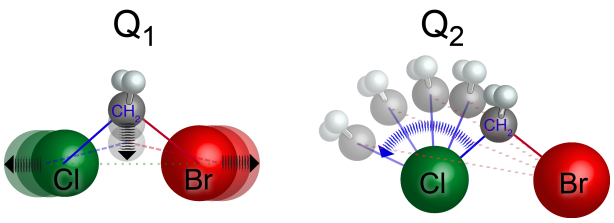

Figure 4: Schematic representation of the dominant nuclear dynamics in the Q_1 and Q_2 normal vibrational modes for CH_2ClBr.

respectively. Figure 3 clearly shows the rotation of the light CH_2 linkage around the Cl atom, while the heavy halogen atoms remain nearly still. Concerning the Cl^+ and Br^+ ions, the predominant variation occurs in the p_y component of their momenta, decreasing towards 0, whereas the p_x projection remains largely unchanged. The case corresponding to alignment of the three ion momenta along the x axis in Fig. 3 indicates the linear geometry resulting from the rotation of the CH_2 group, initially bridging the Cl and Br atoms in the BCM molecule, to the other side of the Cl atom.

For comparison, we also constructed the IPA diagrams for minor sequential dissociation channels (not shown here). In these cases, the momentum distributions of all three ions appear as semi-circles in the IPA frame, revealing notable differences from the dissociation dynamics of the main channel presented in Fig. 3.

By employing ion momentum correlation through the IPA analysis, we can thus depict the dynamics in the primary dissociation pathway for BCM, evoking a mangonel-type catapult. In this analogy, the methylene CH_2 group acts as a projectile while the CH_2–Cl bond serves as a lever arm. Upon X-ray absorption at the Br $3d$ edge, tension builds up in opposing directions along the strongly dissociative Br^*–CH_2 bond, causing the lever arm to release in a radial arc, thereby flinging away the projectile. The experimental data indicates that this bridge, linking the Cl and Br atoms prior to dissociation, is expelled from the molecule, leaving behind the non-bonded Cl-Br ion pair, which undergoes a slower dissociation process while sharing the remaining momentum.

To provide further insights into the nuclear dynamics initiated in the Br $3d$ core-excited

and core-ionized intermediate states, we performed *ab initio* calculations of potential energy surfaces for the ground and intermediate core-hole states. These two-dimensional PESs were described in terms of normal vibrational modes. Analysis of the calculated normal modes showed that only two of them were driving the dissociative dynamics in the core-excited state – Q_1 and Q_2, schematically represented in Fig. 4. Q_1 has a vibrational half-period of 70 fs and is characterized as a heavy vibrational mode involving the $\angle BrCH_2Cl$ bending, where opening of this angle leads to an increase of the Br–Cl distance. In contrast, Q_2 has a vibrational half-period of 26 fs and represents a light mode, primarily associated with the stretching of the Br–CH_2 bond. This mode involves minimal displacement of the halogen atoms and causes only a slight change in the CH_2–Cl internuclear distance, leading to the rotation of the CH_2 group around the Cl atom. The contour plots for the ground, Br $3d$ core-excited, and core-ionized intermediate states are shown in Fig. 5, which also include the simulated time-integrated vibrational wave packets overlaying the corresponding PES landscapes. The theory affirms the dissociative nature of the core-excited state along both Q_1 and Q_2 normal modes, while the core-ionized state is bound with a shallower minimum compared to the ground state. Simulations of nuclear wave-packet propagation using these PESs corroborate extensive dynamics in the core-excited state, with only weak dynamics triggered in the core-ionized state. Dissociative motion along the Q_1 normal mode leads to a decrease of $\angle\alpha_{Cl}$ (Fig. 1a) resulting in a decrease of the energy of the CH_2^+ ion as the molecule approaches a linear geometry, with the CH_2 group positioned between the Cl and Br atoms. Dynamics along the Q_2 normal mode result in an increase of $\angle\alpha_{Cl}$ as the Br–CH_2 bond elongates. Experimental results presented in Fig. 2a indicate that the primary dissociation pathway involves an increase in the angle $\angle\alpha_{Cl}$. This indicates that the light mode Q_2 plays a predominant role in driving the dissociative dynamics of the system. This observation is strongly supported by simulations of nuclear-wave-packet propagation on the corresponding potential energy surfaces (PESs), as shown in Fig. 5.

In conclusion, we used COLTRIMS measurements to study the nuclear dynamics in-

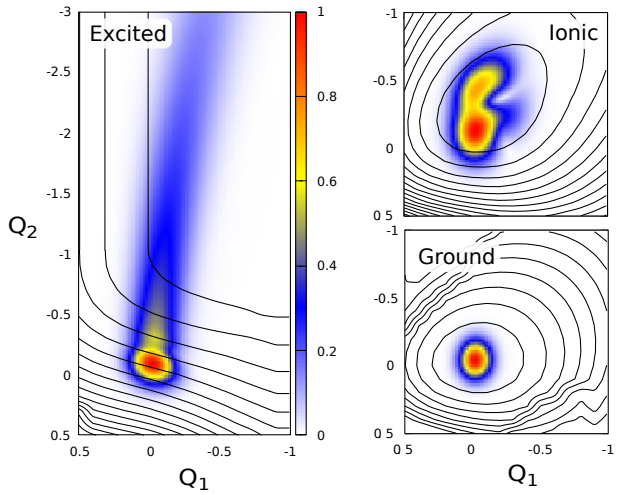

Figure 5: Calculated time-integrated vibrational wave packets in the core-excited (left), core-ionized (top right), and ground (bottom right) states of CH_2ClBr on the top of the corresponding PES landscape, calculated along the selected Q_1 and Q_2 vibrational modes.

volved in the ultrafast dissociation process of strongly repulsive intermediate states of bromochloromethane with a lifetime of only $\tau \sim 7$ fs. To gain deeper insight into the mechanisms driving the primary pathway of three-body dissociation in bromochloromethane, we developed a momentum correlation analysis in the reference frame based on mass-weighted ion pair average (IPA) momenta. This approach effectively incorporates the inherent dynamics of *all* dissociating partners while accounting for substantial differences in their reduced masses, which profoundly influence the overall dynamics. Unlike conventional Newton diagrams, which require fixing the momentum of one particle as a reference, our methodology eliminates this constraint, enabling a more flexible analysis of nuclear dynamics. This approach could prove particularly valuable for understanding non-sequential dissociation mechanisms, where constituent atoms or groups within the molecule dissociate at different times or rates in an asynchronous manner, rather than occurring simultaneously or uniformly. The IPA reference frame could be potentially beneficial for processes characterized by significant differences in ion masses. Through our IPA analysis, we described the primary dissociative channel for bromochloromethane in the Br $3d$ core-excited state, drawing an analogy to a medieval mangonel-type catapult. The experimental data captured the predominant nuclear

motion of the CH_2 moiety and indicated the expulsion of the bridge linking the Cl and Br atoms, which subsequently drift apart over a longer time scale. We observe that this dynamics is significantly attenuated for photon energies above the ionization threshold, where the molecule mainly undergoes concerted dissociation, i.e., the bonds break simultaneously at geometries close to the initial ground-state ones. The conclusions derived from our experimental coincidence data are strongly supported by *ab initio* theoretical calculations. By incorporating vibrational normal modes and performing simulations of nuclear-wave-packet propagation, our calculations provide a comprehensive understanding of the nuclear dynamics triggered by absorption of the soft X-ray photon at the Br $3d$ edge.

Our experimental data and *ab initio* simulations confirm that the presence of light groups between heavy parts of the molecule is crucial for enabling fast nuclear dynamics. The existence of light groups in molecules implies the presence of corresponding low-reduced-mass vibrational modes. In more complex molecular systems, such as those containing longer alkylene or alkenylene groups, several low-reduced-mass vibrational modes combine to collectively drive nuclear dynamics along multimode dissociation, enabling ultrafast nuclear dynamics and, consequently, dissociation on very short time scales.

Methods

Measurements were carried out at the XUV beamline UE112_PGM-1 at the BESSY II electron storage ring operated by the Helmholtz-Zentrum Berlin für Materialien und Energie[33] in the single-bunch timing mode (bunch spacing 800 ns), using photons of 70.3 and 85 eV photon energy generated by its elliptical undulator, with approximately 60 meV photon-energy resolution provided by the monochromator. We used a mobile cold target recoil ion momentum spectroscopy (COLTRIMS) reaction microscope[36–38] for our studies. The CH_2BrCl molecules were provided in a supersonic gas jet, which passed two skimmers (300 μm diameter each) and was crossed with the photon beam at right angle. We used the vapor pressure

of approximately 200 mbar at room temperature and a gas nozzle of 200 μm diameter. The employed COLTRIMS spectrometer consisted of an ion arm of 4 cm acceleration length and an electron arm of 6 cm acceleration and 12 cm drift length (Wiley-McLaren time-of-flight focusing geometry[39]). Both were equipped with a microchannel-plate detector (active area of 80 mm diameter for the electrons and of 120 mm diameter for the ions) with hexagonal delay-line position readout.[40] Electrons and ions were guided by homogeneous electric (15.5 V/cm) and magnetic (12.5 G) fields onto the two time- and position-sensitive detectors. From the times of flight and the positions of impact, the three-dimensional momentum vectors of all charged fragments of the photoreaction were retrieved as well as derived quantities, e.g., kinetic energies and emission angles. All ionic fragments were detected in coincidence with slow electrons. The count rates for triple-ion coincidences at the two different photon energies were approximately proportional to the estimated cross sections for triple ($\sim$2%[34]) and double ($\sim$14%[35]) Auger decays, respectively. Our momentum resolution allowed us to distinguish between the ^{79}Br and ^{81}Br isotopes, the ^{35}Cl and ^{37}Cl isotopes as well as between C^+, CH^+, and CH_2^+. Only the events that fulfil the momentum conservation law were retained in the data analysis. The data, recorded at 70.3 and 85 eV, was normalised to the same integrated count rate before applying filters to extract events associated with the dominant fragmentation pattern.

The normal vibrational modes were calculated for the optimized ground state of BCM using the Hartree-Fock method with the second-order Møller-Plesset correlation energy correction (MP2) with the 6-311+G(d',p') basis set. The two-dimensional potential energy surface (PES) of the initial ground state was first calculated as functions of the Q_1 and Q_2 normal vibrational modes at a post-Hartree-Fock multi-configurational self-consistent field (MCSCF) level of theory as implemented in the GAMESS(US) *ab initio* package. The ten highest doubly occupied molecular orbitals (MOs) and the twenty low-lying vacant MOs were considered into the active space considering single up to double valence excitations. We opted for the strategy of replacing a core hole in the 3*d* orbital with a core hole in the

$3s$ orbital in the theoretical calculations to avoid the complexities introduced by spin-orbit splitting. Since both $3d$ and $3s$ are core orbitals, substituting one for the other minimally impacts the valence electronic structure. Consequently, this substitution has little effect on the description of nuclear dynamics. The two-dimensional potential energy surface of the $3s$ inner-shell threshold of CH_2ClBr, e.g., the $Br(3s^{-1})$ core-ionized state and the low-lying $Br(3s^{-1}V^1)$ (V denotes a vacant molecular orbital) core-excited state were calculated as functions of the Q_1 and Q_2 normal modes combining a restricted open-shell Hartree-Fock approach in order to optimize the molecular orbitals in presence of a core vacancy combined with a post-Hartree-Fock configuration interaction (CI) approach. The CI active space considered for the $Br(3s^{-1})$ [$Br(3s^{-1}V^1)$] core-ionized [core-excited] state takes into account the ten highest doubly occupied MOs and the forty low-lying vacant MOs considering single up to double valence (CI-SD) excitations. A 6-311G++(3*df*,3*pd*) basis set was used for the carbon, chlorine, and hydrogen atoms. A triple zeta valence (TZV) atomic Cartesian-Gaussian basis set with additional (s, p, d) diffuse functions centered on the Br atom was considered. To simulate X-ray-induced dynamics in core-excited and core-ionized states, nuclear wave packets were propagated on the corresponding PESs taking into account the Br $3d$ core-hole lifetime using the time-dependent solution of the two-dimensional Schrödinger equation along the selected Q_1 and Q_2 vibrational modes. The details of the simulations can be found in Refs.[41–43] In the present work, we neglected the weak dependence of the excitation transition dipole moment on the molecular geometry, as the ground-state vibrational wave function is highly localized around the equilibrium position.

Author contributions

OT initially conceptualized the study, with further development by MNP, TJ, RD, and MS. FT, MSS, TJ, and RD designed the experiment. OT, BCM, FT, MSS, GK, and TJ conducted the beam time and acquired the experimental data. BCM performed preliminary

data treatment with assistance from FT and TJ. OT analyzed the data. VK and SC performed calculations. OT wrote the original draft with significant review and editing by VK, FT, TM, and TJ. All authors discussed the results and commented on the manuscript.

Data availability

Data for this article, processed (calibrated and analysed using various data filters), are available at DropSu depository of the Sorbonne University at https://dropsu.sorbonne-universite.fr/s/RDofJcCfjXWiPkT. In case access password is required, it is provided by the corresponding author.

Acknowledgement

We thank the Helmholtz-Zentrum Berlin für Materialien und Energie for the allocation of synchrotron radiation beamtime. BCM and MS acknowledge funding by the French Agence Nationale de la Recherche (ANR) through the SUMMIT project (ANR-13-IS04-0005). FT acknowledges funding by the Deutsche Forschungsgemeinschaft (DFG, German Research Foundation) - Project 509471550, Emmy Noether Programme.

References

(1) Ågren, H.; Nordgren, J.; Selander, L.; Nordling, C.; Siegbahn, K. Valence Electron Structure of the SF_6 and CS_2 Molecules, Studied in High Resolution X-ray Emission. *Phys. Scr.* **1978**, *18*, 499.

(2) Morin, P.; Nenner, I. Atomic Autoionization Following Very Fast Dissociation of Core-Excited HBr. *Phys. Rev. Lett.* **1986**, *56*, 1913.

(3) Menzel, A.; Langer, B.; Viefhaus, J.; Whitfield, S. B.; Becker, U. Competition between

direct dissociation and resonant Auger decay: a quasi-classical model applied to the $2p^{-1}\sigma^*$ states of HCl, DCl and Cl_2. *Chem. Phys. Lett.* **1996**, *258*, 265–270.

(4) Björneholm, O.; Bässler, M.; Ausmees, A.; Hjelte, I.; Feifel, R.; Wang, H.; Miron, C.; Piancastelli, M. N.; Svensson, S.; Sorensen, S. L.; Gel'mukhanov, F.; Ågren, H. Doppler Splitting of In-Flight Auger Decay of Dissociating Oxygen Molecules: The Localization of Delocalized Core Holes. *Phys. Rev. Lett.* **2000**, *84*, 2826.

(5) Hjelte, I.; Piancastelli, M. N.; Fink, R. F.; Björneholm, O.; Bässler, M.; Feifel, R.; Giertz, A.; Wang, H.; Wiesner, K.; Ausmees, A.; Miron, C.; Sorensen, S. L.; Svensson, S. Evidence for ultra-fast dissociation of molecular water from resonant Auger spectroscopy. *Chem. Phys. Lett.* **2001**, *334*, 151–158.

(6) Rosenqvist, L.; Wiesner, K.; Naves de Brito, A.; Bässler, M.; Feifel, R.; Hjelte, I.; Miron, C.; Wang, H.; Piancastelli, M. N.; Svensson, S.; Björneholm, O.; Sorensen, S. L. Femtosecond dissociation of ozone studied by the Auger Doppler effect. *J. Chem. Phys.* **2001**, *115*, 3614–3620.

(7) Wiesner, K.; Naves de Brito, A.; Sorensen, S. L.; Burmeister, F.; Gisselbrecht, M.; Svensson, S.; Björneholm, O. The dynamic Auger–Doppler effect in HF and DF: control of fragment velocities in femtosecond dissociation through photon energy detuning. *Chem. Phys. Lett.* **2002**, *354*, 382–388.

(8) Hjelte, I.; Piancastelli, M. N.; Jansson, C. M.; Wiesner, K.; Björneholm, O.; Bässler, M.; Sorensen, S. L.; Svensson, S. Evidence of ultra-fast dissociation in ammonia observed by resonant Auger electron spectroscopy. *Chem. Phys. Lett.* **2003**, *370*, 781–788.

(9) Kitajima, M.; Ueda, K.; De Fanis, A.; Furuta, T.; Shindo, H.; Tanaka, H.; Okada, K.; Feifel, R.; Sorensen, S. L.; Gel'mukhanov, F.; Baev, A.; Ågren, H. Doppler Effect in Resonant Photoemission from SF_6: Correlation between Doppler Profile and Auger Emission Anisotropy. *Phys. Rev. Lett.* **2003**, *91*, 213003.

(10) Le Guen, K.; Miron, C.; Céolin, D.; Guillemin, R.; Leclercq, N.; Simon, M.; Morin, P.; Mocellin, A.; Björneholm, O.; Naves de Brito, A.; Sorensen, S. L. H_2S ultrafast dissociation probed by energy-selected resonant Auger electron–ion coincidence measurements. *J. Chem. Phys.* **2007**, *127*, 114315.

(11) Travnikova, O.; Sisourat, N.; Marchenko, T.; Goldsztejn, G.; Guillemin, R.; Journel, L.; Céolin, D.; Ismail, I.; Lago, A. F.; Püttner, R.; Piancastelli, M. N.; Simon, M. Subfemtosecond Control of Molecular Fragmentation by Hard X-Ray Photons. *Phys. Rev. Lett.* **2017**, *118*, 213001.

(12) Gel'mukhanov, F.; Odelius, M.; Polyutov, S. P.; Föhlisch, A.; Kimberg, V. Dynamics of resonant x-ray and Auger scattering. *Rev. Mod. Phys.* **2021**, *93*, 035001.

(13) Björneholm, O.; Sundin, S.; Svensson, S.; Marinho, R. R. T.; Naves de Brito, A.; Gel'mukhanov, F.; Ågren, H. Femtosecond Dissociation of Core-Excited HCl Monitored by Frequency Detuning. *Phys. Rev. Lett.* **1997**, *79*, 3150.

(14) Kitajima, M.; De Fanis, A.; Okada, K.; Yoshida, H.; Hoshino, M.; Tanaka, H.; Ueda, K. High-resolution resonant Auger spectroscopy of CF_4, SiF_4, and SF_6. *J. Electron Spectrosc. Relat. Phenom.* **2005**, *144-147*, 199–202.

(15) Miron, C.; Morin, P.; Céolin, D.; Journel, L.; Simon, M. Multipathway dissociation dynamics of core-excited methyl chloride probed by high resolution electron spectroscopy and Auger-electron–ion coincidences. *J. Chem. Phys.* **2008**, *128*, 154314.

(16) Sann, H. et al. Imaging the temporal evolution of molecular orbitals during ultrafast dissociation. *Phys. Rev. Lett.* **2016**, *117*, 243002.

(17) Travnikova, O. et al. Ultrafast dissociation of ammonia: Auger-Doppler effect and redistribution of the internal energy. *Phys. Chem. Chem. Phys.* **2022**, *24*, 5842–5854.

(18) Travnikova, O.; Hosseini, F.; Marchenko, T.; Guillemin, R.; Ismail, I.; Moussaoui, R.; Journel, L.; Milosavljević, A. R.; Bozek, J. D.; Kukk, E.; Püttner, R.; Piancastelli, M. N.; Simon, M. Dynamics of core-excited ammonia: disentangling fragmentation pathways by complementary spectroscopic methods. *Phys. Chem. Chem. Phys.* **2023**, *25*, 1063–1074.

(19) Kukk, E. Nuclear dynamics and electronic structure of molecules by resonant Auger spectroscopy. *J. Electron Spectrosc. Relat. Phenom.* **2002**, *127*, 43–51.

(20) Lago, A. F.; Santos, A. C. F.; de Souza, G. G. B. Mass spectrometry study of the fragmentation of valence and core-shell (Cl 2p) excited $CHCl_3$ and $CDCl_3$ molecules. *J. Chem. Phys.* **2004**, *120*, 9547–9555.

(21) Céolin, D.; Travnikova, O.; Bao, Z.; Kivimäki, A.; Carniato, S.; Piancastelli, M. N. Effect of the Cl2p core orbital excitation on the nuclear dynamics of the three dichloroethylene isomers. *J. Electron Spectrosc. Relat. Phenom.* **2011**, *184*, 24–28.

(22) Kokkonen, E.; Jänkälä, K.; Patanen, M.; Cao, W.; Hrast, M.; Bučar, K.; Žitnik, M.; Huttula, M. Role of ultrafast dissociation in the fragmentation of chlorinated methanes. *J. Chem. Phys.* **2018**, *148*, 174301.

(23) Travnikova, O.; Kimberg, V.; Flammini, R.; Liu, X.-J.; Patanen, M.; Nicolas, C.; Svensson, S.; Miron, C. On Routes to Ultrafast Dissociation of Polyatomic Molecules. *J. Phys. Chem. Lett.* **2013**, *4*, 2361–2366.

(24) Hammerich, A. D.; Manthe, U.; Kosloff, R.; Meyer, H.-D.; Cederbaum, L. S. Time-dependent photodissociation of methyl iodide with five active modes. *J. Chem. Phys.* **1994**, *101*, 5623–5646.

(25) Schinke, R. *Photodissociation dynamics: Spectroscopy and fragmentation of small molyatomic Molecules*; Cambridge Monographs on Atomic, Molecular and Chemical Physics; Cambridge University Press, 1993.

(26) Busch, G. E.; Wilson, K. R. Triatomic photofragment spectra. I. Energy partitioning in NO_2 photodissociation. *J. Chem. Phys.* **1972**, *56*, 3626–3638.

(27) Merrill, W. G.; Crim, F. F.; Case, A. S. Dynamics and yields for $CHBrCl_2$ photodissociation from 215–265 nm. *Phys. Chem. Chem. Phys.* **2016**, *18*, 32999–33008.

(28) Brynteson, M. D.; Womack, C. C.; Booth, R. S.; Lee, S. H.; Lin, J. J.; Butler, L. J. Radical intermediates in the addition of OH to propene: photolytic precursors and angular momentum effects. *J. Phys. Chem. A* **2014**, *118*, 3211–3229.

(29) Schmelz, H. C.; Reynaud, C.; Simon, M.; Nenner, I. Site-selective fragmentation in core-excited bromo-chloro-alkanes $[Br(CH)_2)_nCl]$. *J. Chem. Phys.* **1994**, *101*, 3742–3749.

(30) Neumann, N.; Hant, D.; Schmidt, L. P. H.; Titze, J.; Jahnke, T.; Czasch, A.; Schöffler, M. S.; Kreidi, K.; Jagutzki, O.; Schmidt-Böcking, H.; Dörner, R. Fragmentation Dynamics of CO_2^{3+} Investigated by Multiple Electron Capture in Collisions with Slow Highly Charged Ions. *Phys. Rev. Lett.* **2010**, *104*, 103201.

(31) Williams, J. B.; Trevisan, C. S.; Schöffler, M. S.; Jahnke, T.; Bocharova, I.; Kim, H.; Ulrich, B.; Wallauer, R.; Sturm, F.; Rescigno, T. N.; Belkacem, A.; Dörner, R.; Weber, T.; McCurdy, C. W.; Landers, A. L. Imaging polyatomic molecules in three dimensions using molecular frame photoelectron angular iistributions. *Phys. Rev. Lett.* **2012**, *108*, 233002.

(32) Williams, J. B.; Trevisan, C. S.; Schöffler, M. S.; Jahnke, T.; Bocharova, I.; Kim, H.; Ulrich, B.; Wallauer, R.; Sturm, F.; Rescigno, T. N.; Belkacem, A.; Dörner, R.; Weber, T.; McCurdy, C. W.; Landers, A. L. Probing the dynamics of dissociation of methane following core ionization using three-dimensional molecular-frame photoelectron angular distributions. *J. Phys. B: At. Mol. Opt. Phys.* **2012**, *45*, 194003.

(33) Schiwietz, G.; Beye, M.; Kachel, T. UE112_PGM-1: An open-port low-energy beamline at the BESSY II undulator UE112. *J. Large-Scale Res. Facil.* **2015**, *1*, A33.

(34) Hult Roos, A.; Eland, J. H. D.; Andersson, J.; Wallner, M.; Squibb, R. J.; Feifel, R. Relative extent of triple Auger decay in CO and CO_2. *Phys. Chem. Chem. Phys.* **2019**, *21*, 9889–9894.

(35) Hult Roos, A.; Eland, J. H. D.; Andersson, J.; Squibb, R. J.; Koulentianos, D.; Talaee, O.; Feifel, R. Abundance of molecular triple ionization by double Auger decay. *Sci. Rep.* **2018**, *8*, 16405.

(36) Dörner, R.; Mergel, V.; Jagutzki, O.; Spielberger, L.; Ullrich, J.; Moshammer, R.; Schmidt-Böcking, H. Cold Target Recoil Ion Momentum Spectroscopy: a 'momentum microscope' to view atomic collision dynamics. *Phys. Rep.* **2000**, *330*, 95–192.

(37) Ullrich, J.; Moshammer, R.; Dorn, A.; Dörner, R.; Schmidt, L. P. H.; Schmidt-Böcking, H. Recoil-ion and electron momentum spectroscopy: reaction-microscopes. *Rep. Prog. Phys.* **2003**, *66*, 1463.

(38) Jahnke, T.; Weber, T.; Osipov, T.; Landers, A. L.; Jagutzki, O.; Schmidt, L. P. H.; Cocke, C. L.; Prior, M. H.; Schmidt-Böcking, H.; Dörner, R. Multicoincidence studies of photo and Auger electrons from fixed-in-space molecules using the COLTRIMS technique. *J. Electron Spectrosc. Relat. Phenom.* **2004**, *141*, 229–238.

(39) Wiley, W. C.; McLaren, I. H. Time-of-Flight Mass Spectrometer with Improved Resolution. *Rev. Sci. Instrum.* **1955**, *26*, 1150–1157.

(40) Jagutzki, O.; Cerezo, A.; Czasch, A.; Dörner, R.; Hattaß, M.; Huang, M.; Mergel, V.; Spillmann, U.; Ullmann-Pfleger, K.; Weber, T.; Schmidt-Böcking, H.; Smith, G. D. W. Multiple hit readout of a microchannel plate detector with a three-layer delay-line anode. *IEEE Trans. Nucl. Sci.* **2002**, *49*, 2477–2483.

(41) Ignatova, N.; da Cruz, V. V.; Couto, R. C.; Ertan, E.; Odelius, M.; Ågren, H.; Guimarães, F. F.; Zimin, A.; Polyutov, S. P.; Gel'mukhanov, F.; Kimberg, V. Infrared-

pump–x-ray-probe spectroscopy of vibrationally excited molecules. *Phys. Rev. A* **2017**, *95*, 042502.

(42) Ertan, E.; Savchenko, V.; Ignatova, N.; Vaz da Cruz, V.; Couto, R. C.; Eckert, S.; Fondell, M.; Dantz, M.; Kennedy, B.; Schmitt, T.; Pietzsch, A.; Föhlisch, A.; Gel'mukhanov, F.; Odelius, M.; Kimberg, V. Ultrafast dissociation features in RIXS spectra of the water molecule. *Phys. Chem. Chem. Phys.* **2018**, *20*, 14384–14397.

(43) Vaz da Cruz, V. et al. Probing hydrogen bond strength in liquid water by resonant inelastic X-ray scattering. *Nat. Commun.* **2019**, *10*, 1013.